

Tests and characterization of a laterally graded multilayer Montel mirror

K. Mundboth,^{a*} J. Sutter,^a D. Laundry,^a S. Collins,^a S. Stoupin^b and Y. Shvyd'ko^b

^aDiamond Light Source Ltd, Harwell Science and Innovation Campus, Didcot OX11 0DE, UK, and

^bAdvanced Photon Source, Argonne National Laboratory, Argonne, IL 60439, USA.

*E-mail: kiran.mundboth@diamond.ac.uk

Received 14 February 2013

Accepted 27 August 2013

Multilayers are becoming an increasingly important tool in X-ray optics. The essential parameters to design a pair of laterally graded multilayer mirrors arranged in a Montel-type configuration for use as an X-ray collimating device are provided. The results of X-ray reflectometry tests carried out on the optics in addition to metrology characterization are also shown. Finally, using experimental data and combined with X-ray tracing simulations it is demonstrated that the mirror meets all stringent specifications as required for a novel ultra-high-resolution inelastic X-ray scattering spectrometer at the Advanced Photon Source.

Keywords: X-ray optics; collimating optics; Montel mirrors; laterally graded multilayers; KB mirrors.

© 2014 International Union of Crystallography

1. Introduction

Because of its distinctive design, Montel optics (Montel, 1957) have numerous advantages over traditional Kirkpatrick–Baez (KB) mirrors (Kirkpatrick & Baez, 1948). In contrast to KB systems where the two reflective surfaces are arranged in-line one after the other, those in Montel optics are mounted side by side at 90° to each other (Figs. 1*a* and 1*b*). Due to this fact, the incident X-ray beam now undergoes reflection simultaneously from both surfaces instead of being reflected sequentially as in the KB system. Hence, the mirror-focal point distance is diminished and consequently the demagnification ratio increased. The gain can be substantial especially when the focal distance is comparable with the mirror lengths. Furthermore, the side-by-side geometry offers a more compact design and therefore represents a convenient solution when space availabilities for optical elements are highly restrictive. In terms of mechanical structures, KB optics usually require two independent sets of alignment stages for each mirror. It is possible, in the Montel system, to assemble both surfaces together with their stages onto a common platform. Apart from providing a compact solution, this can also help in reducing the sources of parasitic vibrations as well as any individual misalignment between the mirrors. Lastly, since in this geometry

the second mirror is positioned closer to the source than in the KB system, for the same angular acceptance in both mirror systems, a shorter mirror is needed in the Montel optics design. This is highly desirable as significantly better figure errors can be achieved for smaller mirror sizes than larger ones with the overall benefit of yielding less aberrated beams.

Though Montel optics prove to be particularly beneficial in general (Liu *et al.*, 2011; Ice *et al.*, 2009), for applications where large angular acceptances are essential they might still exhibit shortcomings. For instance, to collect a beam diverging from a point source at a distance of 1 m within a solid angle of

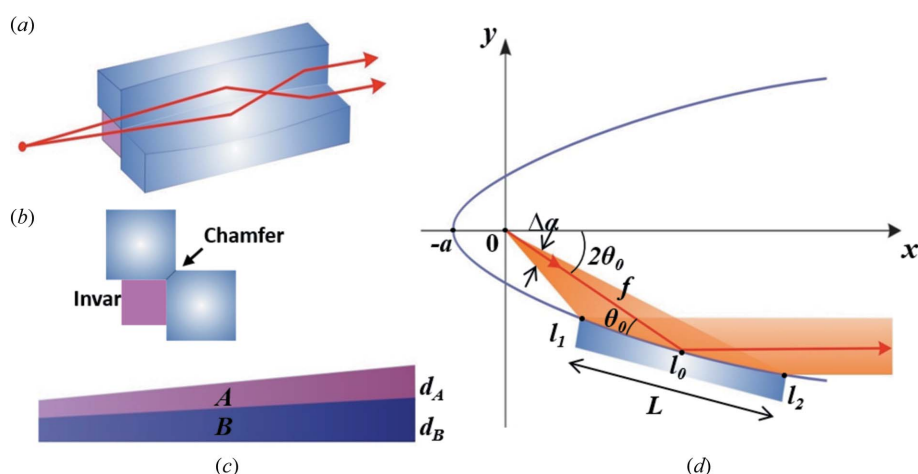


Figure 1 (a) Scheme of the Montel-type optics. Rays are reflected from both surfaces simultaneously unlike KB systems. (b) Side view of the mirror system showing the Invar corner piece and a chamfer along one edge of each mirror surface. (c) Representation of a laterally graded bilayer (A and B) showing the thickness variation from one end to the other. (d) Reflection geometry of a parabolic-shaped mirror.

10 mrad \times 10 mrad and at an incidence angle of 0.20° (critical angle of Si at 9 keV), the Montel optics would need surfaces of more than 2 m in length. This is practically unconceivable. The mirror length is determined by the angle of incidence of the beam, the X-ray source–mirror distance, and the X-ray beam divergence. Since undulator sources usually have relatively small divergences, the significant parameter dictating the mirror size is the beam's angle of incidence. Typically, mirrors are based on total external reflection with critical angles of a few tenths of a degree especially at energies around 10 keV. On the other hand, Bragg reflections occur at significantly higher angles and thus can potentially decrease mirror sizes dramatically. Based on this concept, multilayer optics (Spiller, 1972; Barbee, 1986; Ziegler, 1995) have been developed.

Unlike natural crystals where the lattice parameter is fixed, the thicknesses and materials of the series of layers comprising a multilayer can be tailored to satisfy constraints such as energy, angular divergence and energy bandpass of the incident X-ray beam (Fig. 1c). Thus, this makes multilayers suitable for a wide array of applications both in the soft and hard X-ray regime as beam conditioners such as mirrors and monochromators (Chakraborty, 1991; Bilderback, 1982). Due to their 'crystal-like' nature, another advantage of multilayers is that, with a monochromatic beam, they only reflect when Bragg's condition is satisfied. Thus, this greatly simplifies the alignment of multilayer-based optics. In this article, we present a Montel-type laterally graded multilayer mirror. Its purposes, mirror parameters and design specifications are described. The results of preliminary tests and characterizations are also reported and compared with X-ray tracing simulations. Finally, issues with the Montel-type arrangement are addressed.

2. Design specifications of the Montel mirrors

Owing to the weak excitations involved, the study of vibrational dynamics in matter requires energy resolutions in the meV range. To this end, techniques such as inelastic neutron scattering (INS) and inelastic X-ray scattering (IXS) have been developed; in the latter technique, spectrometers exploiting the dynamical diffraction of perfect crystals in backscattering have been built whereby resolutions of a few meVs have been demonstrated (Graeff & Materlik, 1982; Burkel *et al.*, 1987; Masciovecchio *et al.*, 1996). Since then, IXS spectrometers have continually improved, however, based on the same principle where the incident X-ray beam is back-reflected and the use of large and complex analyser set-ups is common. Recently, a novel ultra-high IXS spectrometer (UHRIX) promising sub-meV energy resolution at medium photon energies (around 10 keV) was proposed (Shvyd'ko *et al.*, 2006) and which furthermore can accommodate all the crystal optics in an in-line scheme (Shvyd'ko *et al.*, 2011); thus discarding the conventional back-reflection geometry. However, the analyser system of such a device still imposes strict conditions on the incoming IXS signal from the sample so as to perform at its best without significant loss in photon flux and deteriorating the energy resolution.

These constraints can be expressed as follows (Shvyd'ko, 2004):

(i) Minimum capture solid angle of the IXS signal for relevant count rates on the detector >10 mrad \times 10 mrad, vertical by horizontal (V \times H);

(ii) Maximum angular divergence of the incoming beam onto the analyser (full width at half-maximum, FWHM) <100 μ rad \times 250 μ rad (V \times H);

(iii) Minimum percentage photon flux in the above solid angle reaching the analyser $\sim 50\%$.

In order to fulfil the second condition, collimating optics can suitably be used between the sample and the analyser. And it is reasonable to confine our choice to reflective optics rather than refractive ones (like lenses) where absorption is considerable. Moreover, since the IXS signal will originate virtually from a point source (*i.e.* scattering occurring from a point of the sample), the use of a paraboloidal-shape mirror stands out as the most sensible option for collimation. Apart from the constraints listed above, there are other restrictions too. For instance, the mirror system is required to fit within an area of 175.3 mm \times 198.2 mm (length by width) and have a focal length of $f = 200$ mm. The latter is defined by the distance between the centre of rotation of the diffractometer (sample position) and the centre of the stage onto which the mirror system can be mounted. The large capture solid angle requirement makes a multilayer mirror the best choice and, considering the limited available space and the fact that paraboloidal surfaces with non-negligible figure errors are extremely difficult to manufacture, a Montel-type geometry for the mirror system seems the most practical solution. Since the Montel optics has two surfaces, each surface has to observe a parabolic shape so as to simulate closely the ideal paraboloidal figure necessary for collimation. However, one has to take into account the large angular spread of the scattering beam impinging on the mirror surfaces. Since we are dealing with a multilayer mirror, Bragg's condition needs to be satisfied along the whole length of the mirror to maintain high overall reflectivity. Therefore, to accommodate the angular spread, the period of the bilayers has to vary along the mirror's length, *i.e.* they must be laterally graded.

Owing to the symmetry of the problem, both mirror surfaces are designed identically. Since we have limited space to fit the mirror (175.3 mm along the beam direction), we assume a maximum mirror length of $L = 120$ mm only so as to allow some space for the mechanical structures that will contain the mirror. The angular acceptance $\Delta\alpha$ of the mirror is estimated by $\Delta\alpha = L \sin \theta_0 / f$ where θ_0 is the Bragg angle at the centre of the mirror segment (Fig. 1d). To satisfy constraint (i), an angular acceptance of $\Delta\alpha = 12$ mrad is considered which therefore yields $\theta_0 = 20$ mrad (1.146°), an angle much larger than in Fresnel reflections.

The bilayer materials A and B are chosen such that the contrast in their electron densities (*i.e.* high- and low- Z elements) is the largest possible while both have small absorption coefficients at the desired X-ray working energy. With these conditions, several material pairs are possible such as (W, Mo, Ni) for A and (C, Si, B₄C) for B . In our case, we

Table 1

Specifications of the laterally graded multilayer Montel mirror.

Among others, the values of the focal length f , parabola parameter a , number of bilayers N , layer thickness ratio γ , mean decrement in the refractive index δ , graded period and Bragg angle at different locations (Fig. 1*d*) along the mirror length d and θ , respectively, are given. All parameters were engineered to fulfil the constraints imposed by the UHRIX spectrometer. Slope errors and surface roughness of the substrate were measured by Zeiss prior to coating.

Coating (W/C)	
Dimensions	120 mm × 20 mm
f	200.0 mm
a	0.08 mm
N	100
$\gamma = d_A/(d_A + d_B)$	0.42
δ	1.81×10^{-5}
Angular acceptance $\Delta\alpha$	12.6 mrad × 12.6 mrad
d_{l_1, l_2}	29.35, 35.55, 41.10 Å
θ_{l_1, l_2}	1.369, 1.146, 1.006°
Substrate (Si)	
Dimensions	120 mm × 20 mm × 20 mm
Slope errors	5.38 μ rad (sagittal) 7.81 μ rad (meridional)
Surface roughness	1.3–1.7 Å

chose W/C over a Si substrate because high reflectivity can be achieved and low interfacial roughness has been reported (Macrander *et al.*, 2000). The number of bilayers N is also an important parameter as it defines the energy resolution and the peak reflectivity of the multilayer. Since here, the multilayer is not intended for use as a monochromator, only the peak reflectivity is to be considered which depends on the number of effective bilayers participating in reflecting the beam. It can be shown (Underwood & Barbee, 1981) that, with our set of parameters, this turns out to be about $N = 100$. With this knowledge and using other geometric considerations (Michaelsen *et al.*, 2000; Morawe *et al.*, 1999) it is then possible to calculate all the parameters essential for the design and fabrication of the mirror. The Si substrates, acquired from Zeiss, were prefigured into the required parabolic shape by mechanical and ion-beam polishing (Gawlitza *et al.*, 2008) whilst they were coated with W/C through magnetron sputtering techniques by Incoatec GmbH (Michaelsen *et al.*, 2000). Both substrates were processed in the same sputter run to ensure a perfect matching of the multilayer coatings. The specifications of the Montel optics are tabulated in Table 1.

A critical issue in the Montel system resides in the assembling procedure of the mirror parts (as in Figs. 1*a* and 1*b*). Because reflection will occur mainly around the regions where the two mirror surfaces meet, *i.e.* along the corner, these are the areas which require the most care. Apart from the fact that they need high-quality polishing, the edges will also have to be nested against each other with as little gap as possible. Otherwise, significant photon loss may result. Moreover, the angle between the two assembled surfaces has to be carefully controlled. As will be shown below, such orthogonal misalignment can severely deteriorate the collimating/focusing capabilities of the Montel-type optics. The method used here to mount the mirrors together consists of using a corner piece to which each mirror part is glued along its side edge (Fig. 1*b*). For the corner piece, Invar (FeNi36) was used due to its low

thermal expansion coefficient; also it can be used as a backbone to fix the whole Montel optics to alignment stages of the experimental set-up. To cater for the orthogonality between the mirrors, each surface contains a chamfer along one side of the edge. The chamfer is 0.5 mm wide and is deliberately made at an angle less than 45° to allow for adjustment of the orthogonal angle.

This assembling technique, due to the almost perfect fit, also presents the advantage of virtually having no gap along the corner. Another technique not requiring the use of a chamfer can be found here (Liu *et al.*, 2011).

3. Metrology measurements

The quality of the image generated by the Montel optics will be affected by the presence of topographical defects on the mirror surfaces. Figure errors and roughness are usually the main factors contributing to image aberrations and blurring, non-uniformity in the beam and even loss in intensity. Especially, slope errors give rise to deviations from the ideal path of the reflected beam and therefore broaden the beam divergence. Since specific conditions have to be met for the UHRIX analyser in terms of incident beam divergence and photon flux, metrology tests were therefore undertaken. Surface characterization of both mirror surfaces was performed using the Diamond-NOM (nanometer optical metrology). Using a system of an autocollimated laser beam being reflected from the surface under test and measuring the deflection of the beam, due to imperfections on the surface, from the ideal position, the slope can be calculated (Alcock *et al.*, 2010). Slope errors can be deduced by calculating the deviations of the slope at each measured point on the surface from its theoretical value. In the case of a parabola, assuming the slope is zero at the centre of the segment, the slope s can be written as

$$s = \frac{dy'}{dx'} = \tan \theta_0 \left[1 - \left(\frac{f}{f + x' \cos \theta_0} \right)^{1/2} \right], \quad (1)$$

where (x', y') are the Cartesian coordinates centred at l_0 (Fig. 2, lower inset). Measurements by the NOM were performed on each surface separately before they were assembled together so that the relevant sections along the long edges (meridional axis) are easily accessible (Fig. 2, upper inset). Compared with the theoretical slope, the general figure of both mirror surfaces (S1, S2) seems identical and abides nicely with that of a parabola except at the extremities of the mirror where no W/C coating is present. Slope errors of $\Delta s^m \simeq 5\text{--}10 \mu$ rad r.m.s. meridionally and $\Delta s^s \simeq 5\text{--}15 \mu$ rad r.m.s. sagittally have been measured for both S1 and S2 (Figs. 3*a* and 3*b*). However, S2 displays a slightly better quality surface than S1 and, since the vertical divergence of the exit beam is more critical, it was mounted as the vertical deflecting surface in the Montel optics. To determine the surface roughness, atomic force microscopy imaging was carried out at various locations on the optics (Figs. 4*a* and 4*b*). Though most measurements along the surfaces edges revealed micro-roughness values ranging from

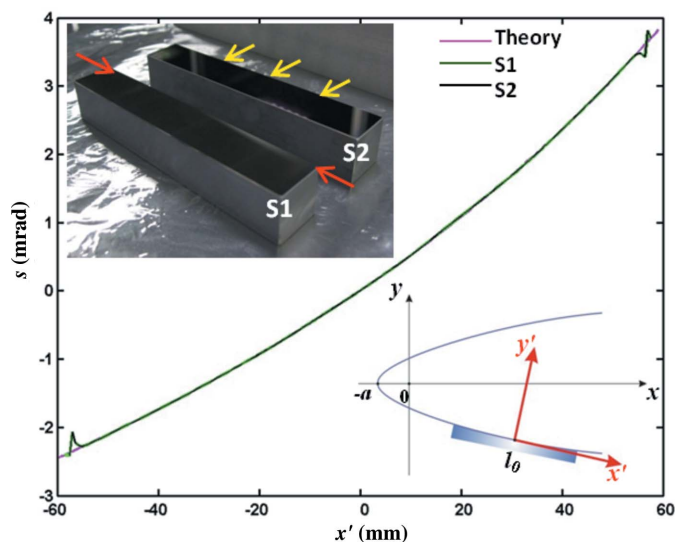


Figure 2 Slope along the surfaces S1 and S2 (meridional axis) of the Montel mirror as indicated by the red arrows in the upper inset. These are compared with the theoretical slope of a parabola calculated for the same mirror segment on the (x', y') Cartesian frame (lower inset). Data were recorded with a step size of 0.5 mm.

1.82 to 2.14 Å, a few trenches have been observed around the central regions (Fig. 4b). Nevertheless, no significant effect on the reflected beam is expected as these portions of the mirror are not exposed to the beam.

4. Reflectivity

The intended use of the Montel mirror is to act as a collimator. However, it can also be employed in reverse and thus be utilized as focusing optics. Whichever way it is used, the reflectivity of the mirror is not affected. To ease the experimental set-up, the reflectivity measurements of the Montel mirror were performed in a focusing geometry, *i.e.* a highly collimated incident beam onto the mirror is focused down to a spot. The former is comfortably provided by a synchrotron beamline and it is more evident, in the focusing configuration, to gauge the performance of the optics as any defects of the mirror will appear as a broadening in the focal spot which is easily perceptible compared with a large beam that would be obtained in a collimating geometry. Moreover, measurement of the size, shape and image quality of the spot allows the figure errors to be estimated through X-ray tracing simulations (these could, therefore, be cross-checked with the results obtained by metrology).

The experiment was carried out at Diamond Light Source Ltd, with a bending-magnet source $55 \mu\text{m} \times 130 \mu\text{m}$ (FWHM) at 46 m from the Montel mirror centre at an energy of $E = 9.13 \text{ keV}$. Slits positioned upstream from the mirror were used to collimate the beam as required. The optics were enclosed in a chamber with He gas and mounted on a goniometer with six degrees (three translations + three rotations) of freedom. A photon diode was used for reflectivity measurements whereas images of the reflected beam were recorded by means of a scintillator + camera system with a spatial resolution as high as

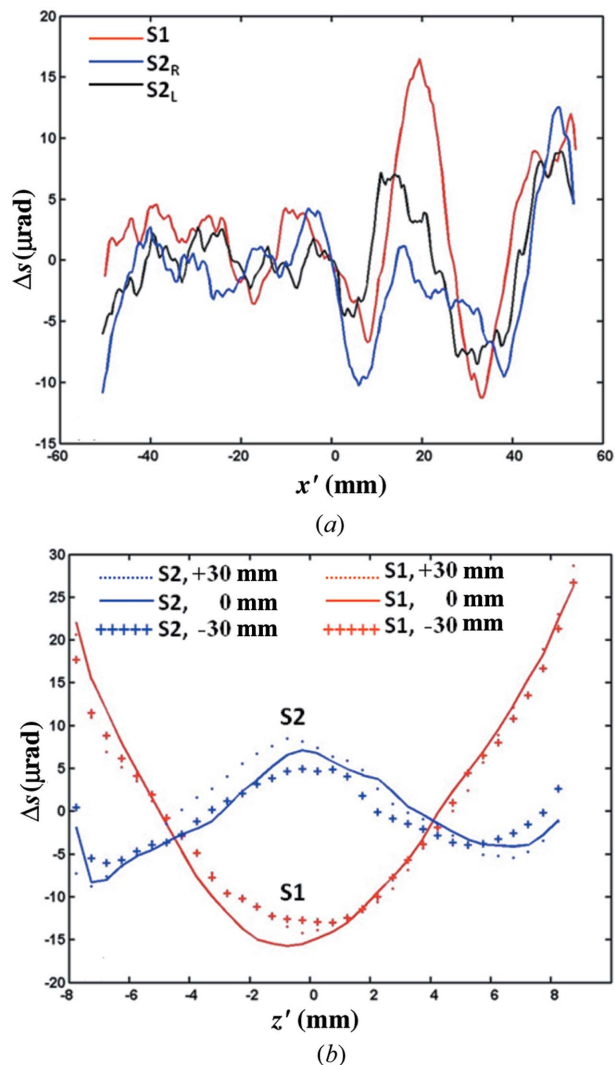


Figure 3 (a) Meridional slope errors along the surfaces S1 and S2 of the Montel mirror as indicated by the red arrows in the upper inset in Fig. 2. Measurements were performed on both right ($S2_R$) and left edges ($S2_L$) of S2. (b) Sagittal slope errors measurements along the directions indicated by the yellow arrows ($x' = 0, \pm 30 \text{ mm}$) in the upper inset in Fig. 2 for both S1 (red curves) and S2 (blue curves) surfaces. Data were recorded with a step size of 0.5 mm.

$0.18 \mu\text{m}$. To avoid measuring the ‘averaged’ reflectivity over the whole optics, each mirror surface is characterized individually and in small sections by slitting down (0.3 mm) the incoming beam creating a beam footprint of about 15 mm onto the mirror. This procedure allows the uniformity along the entire length of each surface to be analysed. The results are presented in Figs. 5(a) and 5(b). Excluding the regions in the vicinity of the mirror extremities, both surfaces manifest consistent peak reflectivities of around 71% with deviations of $< 1.5\%$ from the theoretical Bragg angle. On the other hand, the reduced and shifted peak intensities at the ends of the mirrors hint at a degradation of the coating quality and thickness at these regions. These single reflections, however, do not allow the beam to be focused in both dimensions. For that, both surfaces have to be aligned in which case a doubly reflected beam is obtained; a fine rocking curve of which is

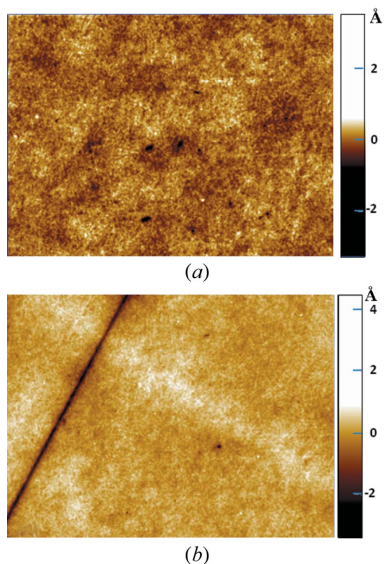


Figure 4 Atomic force microscopy (AFM) images on the mirror surfaces, (a) left edge of S1, (b) central region of S2, within a field of view of $172.9 \mu\text{m} \times 128.6 \mu\text{m}$.

shown in Fig. 5b (inset), where dynamical effects such as an asymmetric curve and oscillations due to the finite thickness of the multilayer can be seen (Authier, 2001). With entrance slits of $0.3 \text{ mm} \times 0.3 \text{ mm}$, a peak reflectivity of around 50% was obtained while a small drop of only 3% was observed when the slits were opened to $1.5 \text{ mm} \times 1.5 \text{ mm}$. The latter slit sizes ensure that the extremities of the mirrors where reduced reflectivity has been measured are masked; hence the observed intensity drop is mainly attributed to the finite size of the Montel optics corner where reflectivity is low. With the above measured values, we can assume that constraint (iii) of the UHRIX analyser is fairly fulfilled.

The focal spot was determined by acquiring a sequence of images along the reflected beam propagation direction (x axis) and determining the smallest focus spot size especially in the vertical direction. This is necessary because the incident beam divergence and the optics figure errors alter the focal length and give rise to astigmatism. With an entrance aperture of $2 \text{ mm} \times 2 \text{ mm}$ so as to illuminate the whole of the Montel optics, an optimal focus spot of $7.6 \mu\text{m} \times 10.7 \mu\text{m}$ ($V \times H$) FWHM is obtained (Fig. 6a), the contribution to the focus size being dominated by slope errors. *A priori*, all the incident beam and mirror parameters are known and therefore can be used to simulate the reflected beam at any position and particularly at the focal length. However, the exact measured profile of the slope errors as determined by metrology characterization cannot be input into the X-ray tracing code such as *RAY* which we used here primarily because it is able to implement laterally graded multilayers. For a given input error value, *RAY* uses a statistical procedure to create a distribution of errors over the whole surface of the optics weighing them with a Gaussian probability function. Therefore this remains as a parameter that requires adjusting in order to produce the same output results as the real surface errors would. After iterative refinement, a suitable match to the experimental

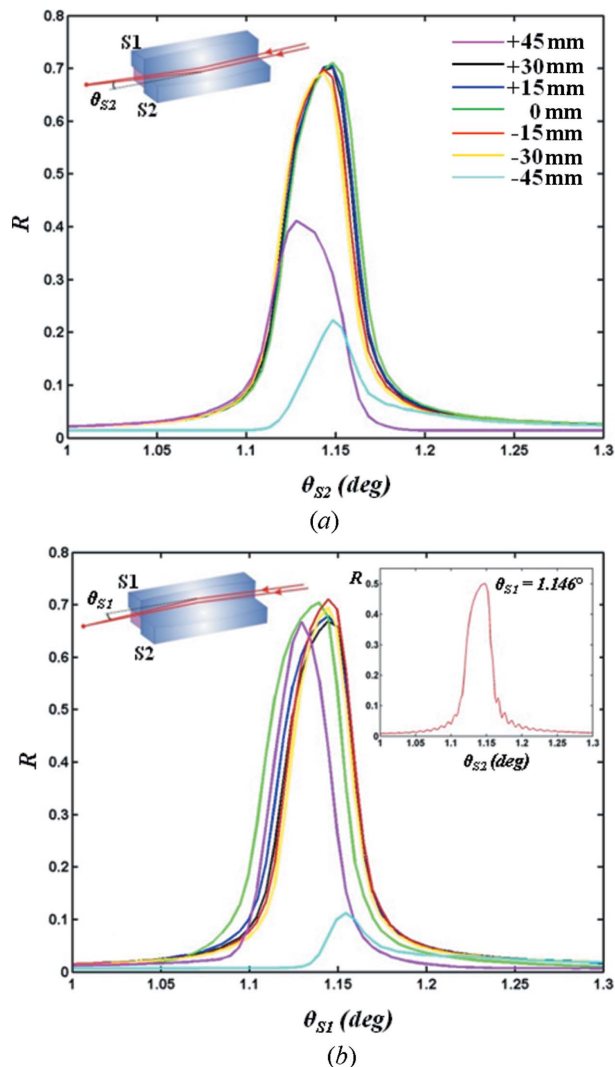


Figure 5 Reflectivity curves recorded in focusing geometry at specific locations on the Montel mirror at about 15 mm intervals along the parabola segment, (a) on S2 and (b) on S1. The top-right inset in (b) shows a fine scan of the reflectivity profile of the doubly reflected beam.

focus spot is obtained (Fig. 6) with meridional slope errors on S1 and S2 such that $\Delta S^{\text{m},S2} = 8.25 \mu\text{rad}$ and $\Delta S^{\text{m},S1} = 11.40 \mu\text{rad}$ which are actually within the range of the measured slope errors (Fig. 3a). In this geometry, sagittal slope errors have insignificant effect on the focus size and are therefore not considered.

5. Effect of orthogonal misalignment

When the entrance aperture is closed down, for instance to $0.1 \text{ mm} \times 0.1 \text{ mm}$, the acquired image exhibits an interesting feature (Fig. 7e); instead of a single focus spot, a double focus spot is revealed. Though appearing obscure, this phenomenon can be explained by understanding the reflection process in Montel optics. As mentioned earlier, in the Montel scheme, reflection occurs from both mirror surfaces simultaneously; consequently, two different pathways for the reflected beam are realised. Some rays are reflected from S1 first before

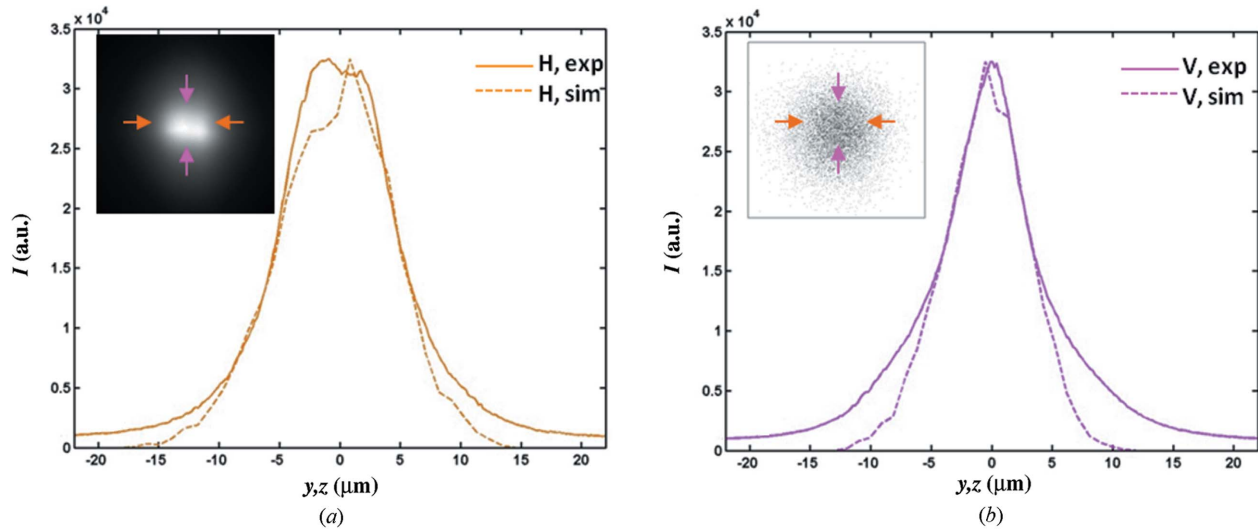


Figure 6 (a) Horizontal (orange) and (b) vertical (magenta) beam profiles of the doubly reflected beam when the Montel mirror is fully illuminated through an entrance slit of 2 mm × 2 mm obtained from both experimental data (exp) and X-ray tracing simulation (sim). The focus spots in each case are shown in the insets; the beam profiles were extracted as indicated by the arrows. The simulated intensities have been normalized to that of the measured data.

impinging on S2 while the remaining rays are reflected in the other order. Both routes are symmetric about the virtual axis contained in the beam that ought to be reflected from the mirror's corner and therefore will intersect the image plane at different points in space; thus producing two spots. The angle χ between the mirror surfaces determines the positions and separation of the spots. In particular, they can be made to overlap when the surfaces are orthogonal to each other while any deviation from orthogonality will move the spots away from each other. One can expect the same effect to occur when the optics are used in the collimating geometry; that is, the formation of two collimated beams shifted from each other. Therefore, this misalignment is a critical point to consider as it creates additional divergence to the non-perfectly collimated beam exiting the mirror. The greater the misalignment, the bigger the divergence and thus the more detrimental to the UHRIX analyser. Hence, it is essential to assess the degree of the misalignment of the reflecting surfaces in the Montel optics.

The double focus spot shown in Fig. 7(e) can be reproduced by simulating both X-ray pathways from which it originates. The results are presented in Figs. 7(a) and 7(b) with pathways S1S2 (S1 is hit first, then S2) and S2S1,

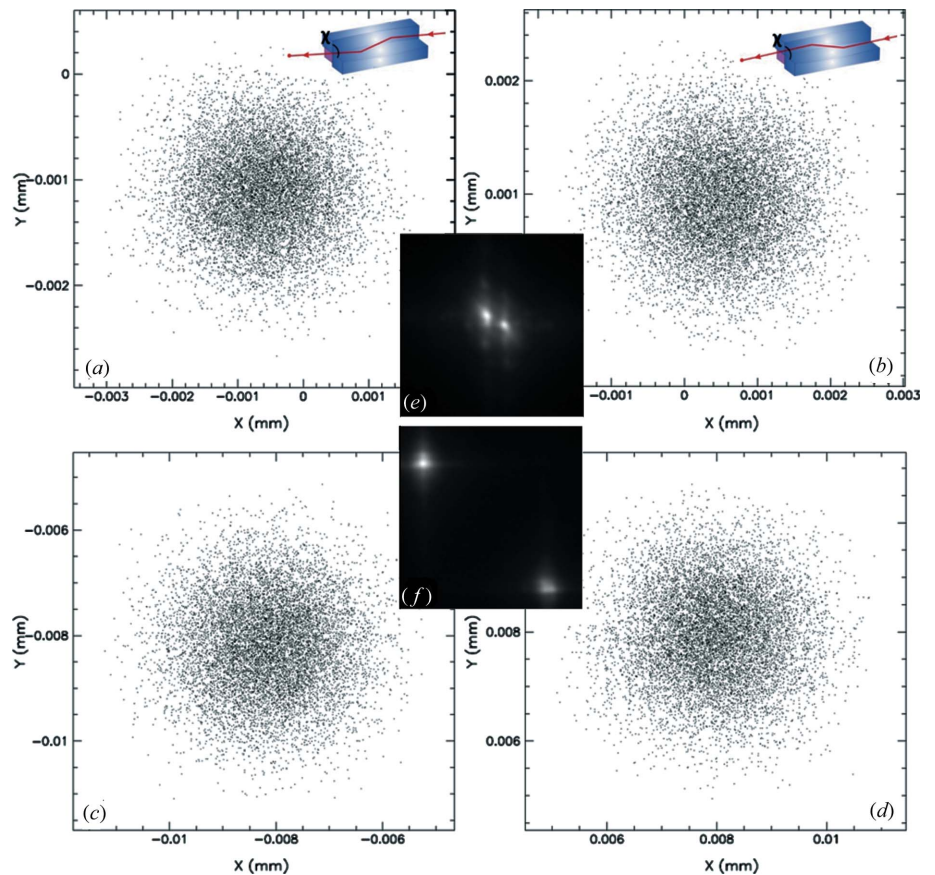


Figure 7 Double spot formation due to misalignments in the orthogonal angle between the two mirror surfaces. (a) and (c) were simulated at $\chi = 90.011^\circ$ and $\chi = 90.115^\circ$, respectively, via pathway S1S2 [inset in (a)]. Same simulations repeated for (b) and (d) via pathway S2S1 [inset in (b)]. Real images of the double spot are shown (f) before and (e) after improving the orthogonality between the mirror surfaces. The entrance aperture was 0.1 mm × 0.1 mm in (e) while it was 0.3 mm × 0.3 mm in (f).

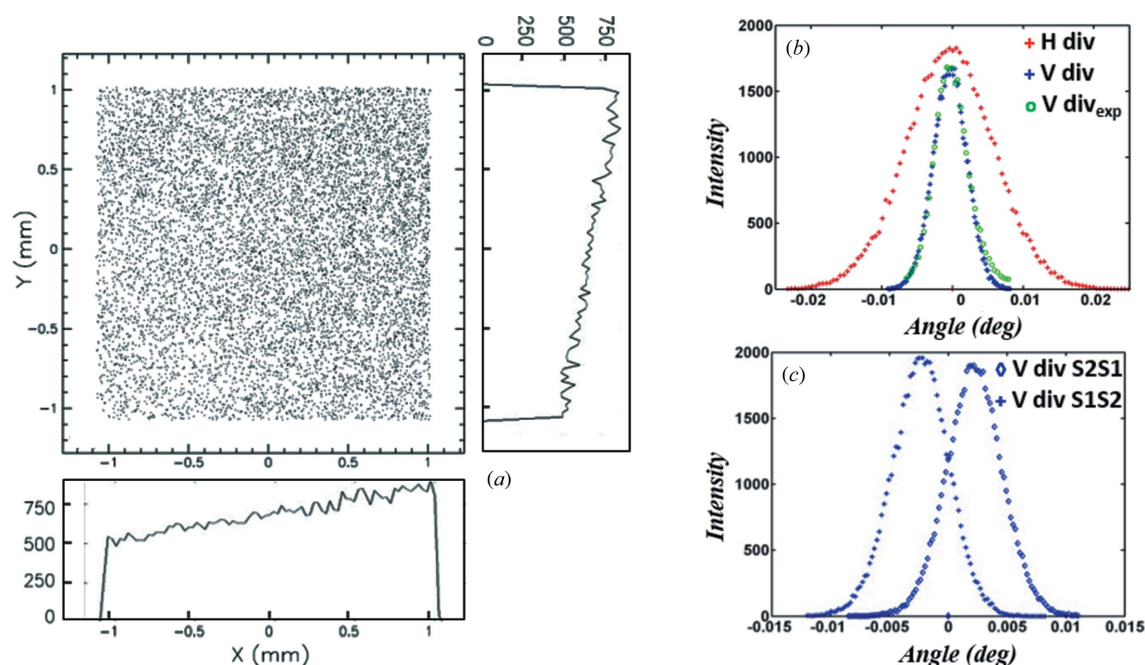


Figure 8

(a) Simulated image of the collimated beam. The integrated number of rays along each axis is indicated on the side panels. (b) Horizontal (red) and vertical (blue) simulated divergences of the collimated beam when $\chi = 90.011^\circ$; (green) vertical divergence of the collimated beam experimentally measured (intensities have been normalized). (c) Vertical divergences of the collimated beam along pathways S1S2 and S2S1 when $\chi = 90.115^\circ$. An additional divergence of about $87 \mu\text{rad}$ is introduced due to the shift between the two beams. The same gap is observed in the horizontal divergences (not shown).

respectively. To obtain a suitable match to the double spot (in terms of distance between them), a misalignment of only $\Delta\chi = 0.011^\circ$ between S1 and S2 was necessary to form the two spots at symmetric coordinates of $(-0.0005, -0.001)$ and $(0.0005, 0.001)$ in the image plane; that is, a separation of only $2.2 \mu\text{m}$ (Fig. 7e). This result was obtained after the Montel optics were modified by the manufacturer with the two surfaces re-assembled; a remarkable improvement compared with its previous misalignment where the distance between the two spots was found to be $23 \mu\text{m}$ (Fig. 7f). In that previous case, a significant deviation of $\Delta\chi = 0.115^\circ$ was estimated through simulations (Figs. 7c and 7d). The two surfaces of our optics are strongly glued to each other so that it is very difficult to eliminate completely the orthogonal error. For that, the mirror surfaces would require to be independent from each other with separate alignment stages very much like in the KB system resulting in a more complex and cumbersome set-up. It is noteworthy that the double spot can only be seen if the individual dimensions of each spot are comparable with their separation. This takes place when the entrance aperture is made sufficiently small to only partly illuminate the optics so that the effect of slope errors is minor. When the aperture is made large such as $2 \text{ mm} \times 2 \text{ mm}$, the focus spots are much larger due to aberrations and they overlap each other so that only one spot is seen as in Fig. 6(a).

Knowing the angle χ between the mirror surfaces, we are now equipped with the whole set of parameters to trace the rays in the collimating geometry and thus obtain the characteristics such as size, shape and divergence of the beam that will be incident on the UHRIX analyser. The ray-trace was

performed with a capture angle of $\Delta\alpha = 11.28 \text{ mrad} \times 11.28 \text{ mrad}$ and meridional slope errors of $\Delta S^{m,S2} = 8.25 \mu\text{rad}$ and $\Delta S^{m,S1} = 11.40 \mu\text{rad}$. These affect the exit divergence of the beam; however, the biggest contribution is given by the source size (the effect of the focal length was found to be insignificant within $\pm 3 \text{ mm}$ from its ideal value of $f = 200 \text{ mm}$). Assuming the latter to be $\Delta s = 18 \mu\text{m} \times 50 \mu\text{m}$ (FWHM, $V \times H$) and with the above parameters, an exit beam size of $2 \text{ mm} \times 2 \text{ mm}$ (Fig. 8a) with a divergence of $98 \mu\text{rad} \times 251 \mu\text{rad}$ ($V \times H$) (Fig. 8b) is obtained. This can be compared with the experimentally measured exit vertical divergence of the Montel optics whereby a striking match is clearly visible between the two curves. The experiment was carried out at the Advanced Photon Source (APS), sector 34 ID beamline during a test beam time of the UHRIX spectrometer with the Montel optics operating as collimator (Shvyd'ko, 2011; Shvyd'ko *et al.*, 2013). The Montel mirrors were illuminated by an elastic scatterer having similar size and located at a focal distance as simulated above, whereas the exit vertical beam divergence was recorded *via* a Si(220) channel-cut and an avalanche photodiode. The above results suggest that the $\Delta\chi$ value of 0.011° deduced from simulations is correct since the other experimental parameters are similar to the simulated ones.

Hence, constraint (ii) is therefore satisfied and thus all the demands of the UHRIX spectrometer have been met. Because $\Delta\chi$ was small in this case, the two pathways S1S2 and S2S1 resulted in a negligible shift between the two collimated beams with no extra divergence. However, if the orthogonality of the Montel optics had not been improved (*i.e.* $\Delta\chi = 0.115^\circ$), then,

with the same parameters as before, the resultant divergences both in the horizontal and vertical directions would have exceeded, with respect to constraint (2), by about 87 μrad (Fig. 8c) due to the formation of two non-overlapping collimated beams propagating away from each other.

6. Conclusion

Characterization of the Montel system yielded excellent results. The tests carried out in both focusing and collimating geometries have shown that it can be used as a very effective collimating device for the UHRIX spectrometer since all specifications in terms of angular acceptance, reflectivity and exit divergence have been met and which moreover agree satisfactorily with simulated results. It is therefore expected that the Montel optics will act as an important tool in future high-resolution IXS studies. Nevertheless, for the collimator to operate satisfactorily, the required source size must be kept small, particularly in the vertical direction ($\Delta s = 18 \mu\text{m} \times 50 \mu\text{m}$, $V \times H$). So special attention needs to be taken in that regard because the performance of the Montel optics could easily be deteriorated. In practice, the optics could also be used as a focusing mirror and, since it has a very compact design, it can fit easily in many different beamlines for numerous potential micro-focusing applications.

The authors would like to thank S. Alcock and G. Ludbrook for carrying out the metrology measurements of the Montel optics as well as the B16 beamline staff for their help during the experiments. The 34-ID beamline staff are acknowledged for providing valuable technical support during the many beam times at the APS.

References

- Alcock, S., Sawhney, K., Scott, S., Pedersen, U., Walton, R., Siewert, F., Zeschke, T., Senf, F., Noll, T. & Lammert, H. (2010). *Nucl. Instrum. Methods Phys. Res. A*, **616**, 224–228.
- Authier, A. (2001). *Dynamical Theory of X-ray Diffraction*. Oxford University Press.
- Barbee, T. W. Jr (1986). *Opt. Eng.* **25**, 898–915.
- Bilderback, D. (1982). *Nucl. Instrum. Methods Phys. Res.* **195**, 67–72.
- Burkel, E., Peisl, J. & Dorner, B. (1987). *Europhys. Lett.* **3**, 957–961.
- Chakraborty, P. (1991). *Int. J. Mod. Phys. B*, **5**, 2133–2228.
- Gawlitza, P., Braun, S., Dietrich, G., Menzel, M., Schädlich, S. & Leson, A. (2008). *Proc. SPIE*, **7077**, 707703.
- Graeff, W. & Materlik, G. (1982). *Nucl. Instrum. Methods Phys. Res.* **195**, 97–103.
- Ice, G. E., Pang, J. W. L., Tulk, C., Molaison, J., Choi, J.-Y., Vaughn, C., Lytle, L., Takacs, P. Z., Andersen, K. H., Bigault, T. & Khounsary, A. (2009). *J. Appl. Cryst.* **42**, 1004–1008.
- Kirkpatrick, P. & Baez, A. V. (1948). *J. Opt. Soc. Am.* **38**, 766–774.
- Liu, W., Ice, G. E., Assoufid, L., Liu, C., Shi, B., Khachatryan, R., Qian, J., Zschack, P., Tischler, J. Z. & Choi, J.-Y. (2011). *J. Synchrotron Rad.* **18**, 575–579.
- Macrander, A., Liu, C., Csencsits, R., Cook, R., Kirk, M. & Headrick, R. (2000). *Physica B*, **283**, 157–161.
- Masciovecchio, C., Bergmann, U., Krisch, M., Ruocco, G., Sette, F. & Verbeni, R. (1996). *Nucl. Instrum. Methods Phys. Res. B*, **111**, 181–186.
- Michaelsen, C., Ricardo, P., Anders, D., Schuster, M., Schilling, J. & Göbel, H. (2000). *Adv. X-ray Anal.* **42**, 308.
- Montel, M. (1957). *X-ray Microscopy with Catamorphic Roof Mirrors, X-ray Microscopy and Microradiography*. New York: Academic Press.
- Morawe, C., Pecci, P., Peffen, J. C. & Ziegler, E. (1999). *Rev. Sci. Instrum.* **70**, 3227.
- Shvyd'ko, Yu. V. (2004). *X-ray Optics—High-Energy-Resolution Applications*, Vol. 98. Springer/Berlin/Heidelberg/New York: Optical Sciences.
- Shvyd'ko, Yu. V. (2011). arXiv:1110.6662v1.
- Shvyd'ko, Y. V., Lerche, M., Kuetgens, U., Rüter, H. D., Alatas, A. & Zhao, J. (2006). *Phys. Rev. Lett.* **97**, 235502.
- Shvyd'ko, Y., Stoupin, S., Mundboth, K. & Kim, J. (2013). *Phys. Rev. A*, **87**, 043835.
- Shvyd'ko, Yu. V., Stoupin, S., Shu, D. & Khachatryan, R. (2011). *Phys. Rev. A*, **84**, 053823.
- Spiller, E. (1972). *Appl. Phys. Lett.* **20**, 365.
- Underwood, J. H. & Barbee, T. W. (1981). *Appl. Opt.* **20**, 3027–3034.
- Ziegler, E. (1995). *Opt. Eng.* **34**, 445–452.